MENISCUS PROFILE IN THE MOLD OF A STEEL CONTINUOUS CASTER

Raúl Miranda, Jesús González, Luis Hoyos, Antonio de Ita, Miguel A. Barrón*
División de Ciencias Básicas e Ingeniería
Universidad Autónoma Metropolitana Azcapotzalco
Apdo. Postal 16-137, C.P. 02011, México, D.F., México
*Fax +( )5318-9474, e-mail bmma@correo.azc.uam.mx

ABSTRACT
Meniscus profile of molten steel in the mold of a slab continuous caster is analyzed in this work by means of physical and numerical simulations. In the physical simulations a one-third scale water model was employed to carry out experiments in which the influence of the water flow rate and the immersion depth of the entry nozzle was investigated. Meniscus profile was tracked employing ultrasonic level sensors located at six different positions along the mold wide walls. In the numerical simulations, computational fluid dynamics software was employed to characterize the flow of molten steel inside the mold. A good qualitative agreement between physical and numerical simulations is obtained. The results are discussed in order to find the optimal position of the mold level sensor in industrial casters.

Keywords: continuous casting, meniscus profile, mold flow.

1. INTRODUCTION
Nowadays continuous casting is the world dominant technology for the production of raw steel. In the continuous casting process (Figure 1), molten steel from a tundish is poured into a copper mold with water-cooled walls through a submerged entry nozzle (SEN). A thin solid shell is formed in the mold walls, which is strong enough to support the remaining molten steel once the product is extracted from the mold. The liquid core of the product is solidified by water sprays located under the mould and cut at the desired length. In the mold, the molten steel surface is covered with a layer of molten flux which acts as thermal insulator and lubricant. Due to the turbulent nature of the flow of molten steel in the mold, permanent oscillations in the steel surface, namely the meniscus, are present. The frequency and amplitude of these oscillations depend on factors such as the chaotic behavior of the turbulent flow, the steel Reynolds number, the casting speed, the molten steel swirl at the outlet ports of the SEN, the mold dimensions, and the SEN design.
On the other hand, industrial casters must maintain the molten steel level as constant as possible given that strong oscillations in the surface of molten steel are responsible of slag emulsification, which causes significant uncleanliness of the solid product [1]. The level sensor must send the right signal to the process computer, which automatically regulates the mold level by adjusting the position of the sliding-gate valve or the casting speed. In recent years, a lot of research work has been carried out at industries and universities in order analyze the meniscus behavior [2-4]. The present authors have studied the meniscus dynamic performance in order to find the optimal position of the sensor level in the mold [5]. Currently, the molten steel flow in the mold and the meniscus profile are investigated either by physical modeling or by numerical simulations. Physical modeling implies the construction of a scale plastic model in which water is used instead of molten steel. However, in order the results of the water model experiments can be extrapolated to the industrial steel caster, the water model must be designed and constructed in accordance with certain similarity criteria. Numerical simulations implies the computer solution of the Navier-Stokes equations and the mass-balance equation. Besides, if the fluid Reynolds number is high, a turbulence model must be solved. In this work, both approaches are employed: a one-third scale plastic water model, and a commercial computational fluid dynamics (CFD) software.

2. PHYSICAL MODELING
A plastic one-third scale water model was designed and constructed in accordance with the Froude similarity criterion. Froude criterion guarantees that the water model is similar to the industrial caster mold from the geometrical and dynamical point of view [6]. The dimensions of the water model are as follows: height 1.20 m, width 0.50 m, thickness 0.08 m. The SEN has two outlet ports with a diameter of 0.02 m, an inlet hole with a diameter of 0.0254 m, and a height of 0.20 m. The outlet port angle is 15°. Water volumetric flow rates were varied from 3.5×10^{-4} to 5.83×10^{-4} m^3 s^{-1}, which correspond to casting speeds from 0.9 to 2.5 m min^{-1}.SEN submergence depth were changed from 0.05 to 0.09 m, as is shown in Table 1. In order to track the transient behavior of the meniscus, six ultrasonic level sensors were located along the wide walls of the water model, as is shown in Figure 2. The signals of the level sensors were recorded in a computer by means of a National Instruments DAQCard-6062E data acquisition card at a rate of 10 samples per second during 15 min extent experiments. This means that 9000 data samples were collected for each sensor.

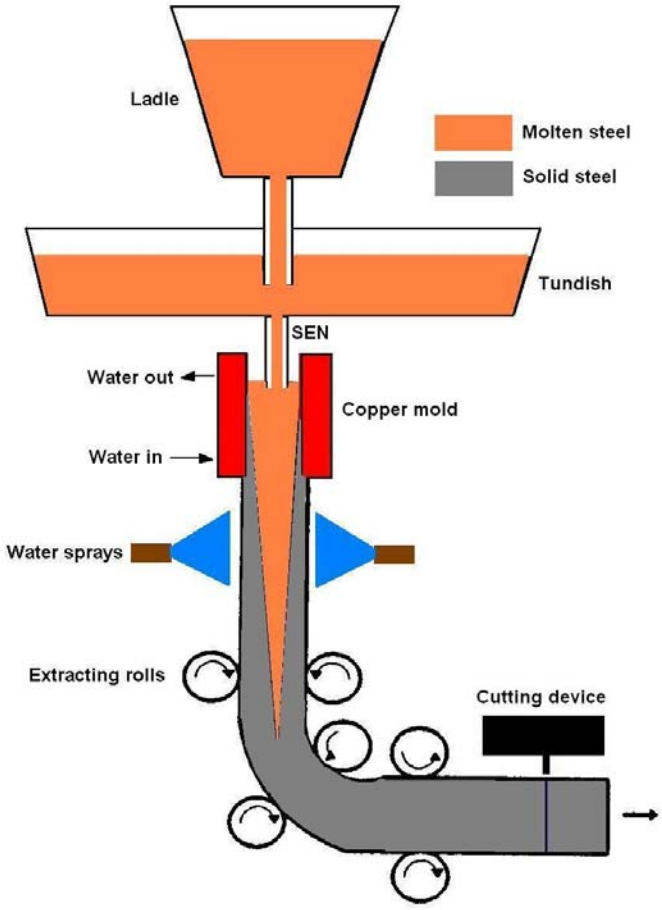

Figure 1. The continuous casting process.

Table 1. Experimental conditions

Case	Water flow rate ($m^3\ s^{-1}$)	SEN submergence depth (m)
1	3.50×10^{-4}	0.050
2	4.67×10^{-4}	0.050
3	5.83×10^{-4}	0.050
4	3.50×10^{-4}	0.070
5	4.67×10^{-4}	0.070
6	5.83×10^{-4}	0.070
7	3.50×10^{-4}	0.090
8	4.67×10^{-4}	0.090
9	5.83×10^{-4}	0.090

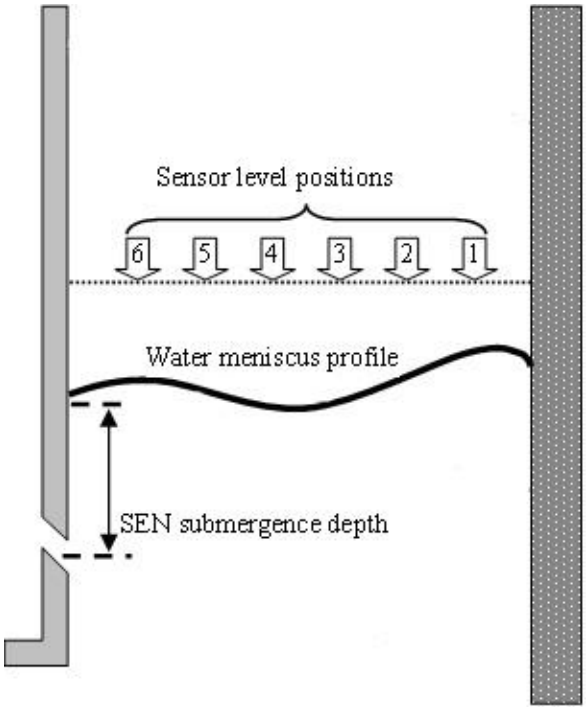

Figure 2. Location of the ultrasonic level sensors in the water model.

3. MATHEMATICAL MODELING

The flow of an incompressible fluid is described by the Navier-Stokes equations. For a two-dimensional system the above equations are expressed as follows [7]:

$$\rho\left(\frac{\partial v_x}{\partial t}+v_x\frac{\partial v_x}{\partial x}+v_y\frac{\partial v_x}{\partial y}\right)=-\frac{\partial p}{\partial x}+\mu\left(\frac{\partial^2 v_x}{\partial x^2}+\frac{\partial^2 v_x}{\partial y^2}\right)+\rho g_x \tag{1}$$

$$\rho\left(\frac{\partial v_y}{\partial t}+v_x\frac{\partial v_y}{\partial x}+v_y\frac{\partial v_y}{\partial y}\right)=-\frac{\partial p}{\partial_y}+\mu\left(\frac{\partial^2 v_y}{\partial x^2}+\frac{\partial^2 v_y}{\partial y^2}\right)+\rho g_y \tag{2}$$

In the above equations ρ is the fluid density, μ is the fluid viscosity, v_x is the x component of the velocity vector, v_y is the y component of the velocity vector, p is the pressure, g_x is the x component of the gravity acceleration vector, g_y is the y component of the gravity acceleration vector, t is the time, and x and y are the system coordinates, respectively. In order to maintain the mass balance in the system, also the continuity equation must be solved [7]:

$$\frac{\partial\rho}{\partial t}+\frac{\partial(\rho v_x)}{\partial x}+\frac{\partial(\rho v_y)}{\partial y}=0 \tag{3}$$

Given that the experiments are carried out isothermally, the energy equation is not considered. However, due to the turbulent of the water flow in the plastic and the molten steel flow in the industrial caster mold, a turbulence model must be employed in order to capture the dynamic flow behavior. The k-ε turbulence model was selected for mathematical modeling, which is described by the following expressions [8]:

$$\frac{\partial}{\partial t}(\rho\kappa)+\frac{\partial}{\partial\xi_i}(\rho\kappa v_i)=\frac{\partial}{\partial\xi_j}\left[\left(\mu+\frac{\mu_t}{\sigma_\kappa}\right)\frac{\partial\kappa}{\partial\xi_j}\right]+G_\kappa+G_b-\rho\varepsilon-Y_M+S_k \tag{4}$$

$$\frac{\partial}{\partial t}(\rho\varepsilon)+\frac{\partial}{\partial \xi_i}(\rho\varepsilon v_i)=\frac{\partial}{\partial \xi_j}\left[\left(\mu+\frac{\mu_t}{\sigma_\varepsilon}\right)\frac{\partial \varepsilon}{\partial \xi_j}\right]+C_{1\varepsilon}\frac{\varepsilon}{\kappa}\left(G_k+C_{3\varepsilon}G_b\right)-C_{2\varepsilon}\rho\frac{\varepsilon^2}{k}+S_\varepsilon \quad (5)$$

In the above equations k is the turbulent kinetic energy, ε is the dissipation rate, v_i is the i component of the velocity vector, G_κ is the generation of kinetic turbulent energy due to mean velocity gradients, G_b is the generation of kinetic turbulent energy due to buoyancy forces, Y_M is the fluctuating dilatation in compressible turbulence to the overall dissipation rate. $C_{1\varepsilon,}$, $C_{2\varepsilon}$ and $C_{3\varepsilon}$ are constants, σ_κ y σ_ε are the turbulent Prandtl number for k and ε, respectively. Besides, S_κ y S_ε are source terms. Finally, t is the time and ξ_i represents the i coordinate of the system.

The fluid viscosity must be corrected for turbulence in the Navier-Stoke equations employing an effective viscosity $\mu_{eff} = \mu_l + \mu_t$, where μ_l is the laminar viscosity and μ_t is the turbulent viscosity. The latter can be determined as follows:

$$\mu_t=\rho C_\mu\frac{\kappa^2}{\varepsilon} \quad (6)$$

where C_μ is a constant.

A commercial computational fluid dynamics (CFD) software called Fluent was employed for numerical solving of the above mathematical model. A two-dimensional mesh with 32500 nodes was created with a time step of 0.001 s. A Dell personal computer with 1 Gb RAM memory, a Pentium 4 3.0 GHz CPU was utilized for the numerical simulations. A run for 70 s of real time required a CPU time of approximately 5 hrs. In order to track the meniscus profile, two-phase flow was considered and the Volume-of-fluid (VOF) model [9] was chosen for tracking of the air-water interface.

4. DISCUSSION OF RESULTS

In Figures 3,4 and 5 are shown the experimental meniscus profiles for Cases 3, 7 and 9 of Table 1, respectively, for each sensor position (see Figure 2). The square in the diamond center is the geometric mean of the 9000 data samples. The line in the middle part of the diamond represents the data median, whereas the lower and upper corners correspond to the 25th and 75th percentiles. The inverted triangles represent the 99th percentiles, and the upper-filled circles correspond to the highest value of the data samples. Besides, the right triangles represent the 1th percentiles, and the lower-filled circles correspond to the lowest value of the data samples.

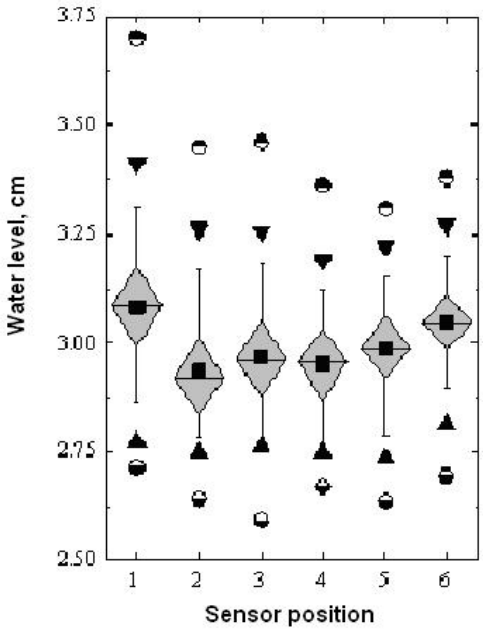

Figure 3. Experimental results for Case 3.

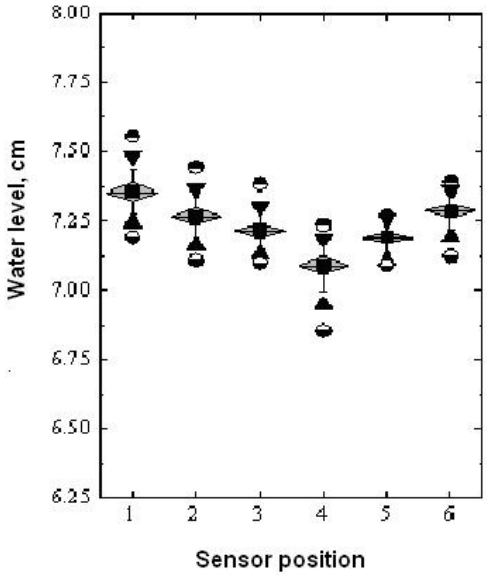

Figure 4. Experimental results for Case 7.

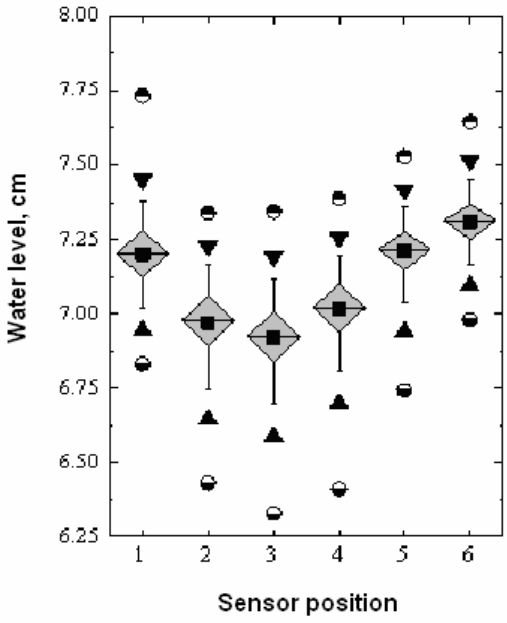

Figure 5. Experimental results for Case 9.

Numerical simulation results are shown in the next figures. Figure 6 illustrates the four-roll typical flow pattern in a continuous casting mold. The water jets exit the SEN outlet ports with a 15° angle and bifurcate just before the mold narrow walls. Two recirculation rolls are formed in the upper part of the mold, and two recirculation rolls are formed in the lower region of the mold. Besides, it can be seen the flow lines toward the exit nozzle located in the bottom of the water model.

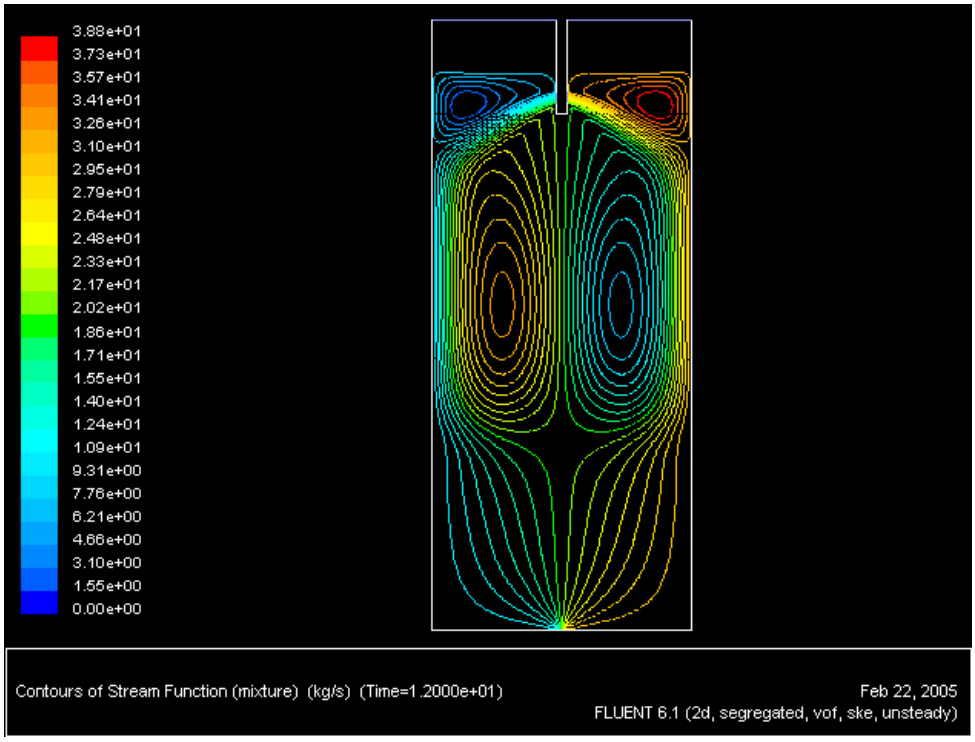

Figure 6. Contours of stream function for Case 3.

Figure 7 shows the velocity vector distributions in the upper region of the water mold. The highest velocities are located in the water jets emerging from the SEN outlet ports. In the meniscus zone the horizontal component of the velocity is predominant and here the flow is directed towards the SEN, both in the left and the right sides of the mold. The upper recirculation flows are responsible of the meniscus oscillations. Eventually, if the amplitude of the meniscus oscillations in the real steel caster is significant, molten flux above the steel surface becomes emulsified and slag entrapment in the steel may occur. Of course, this causes undesirable uncleanliness in the solid steel which yields poor mechanical properties.

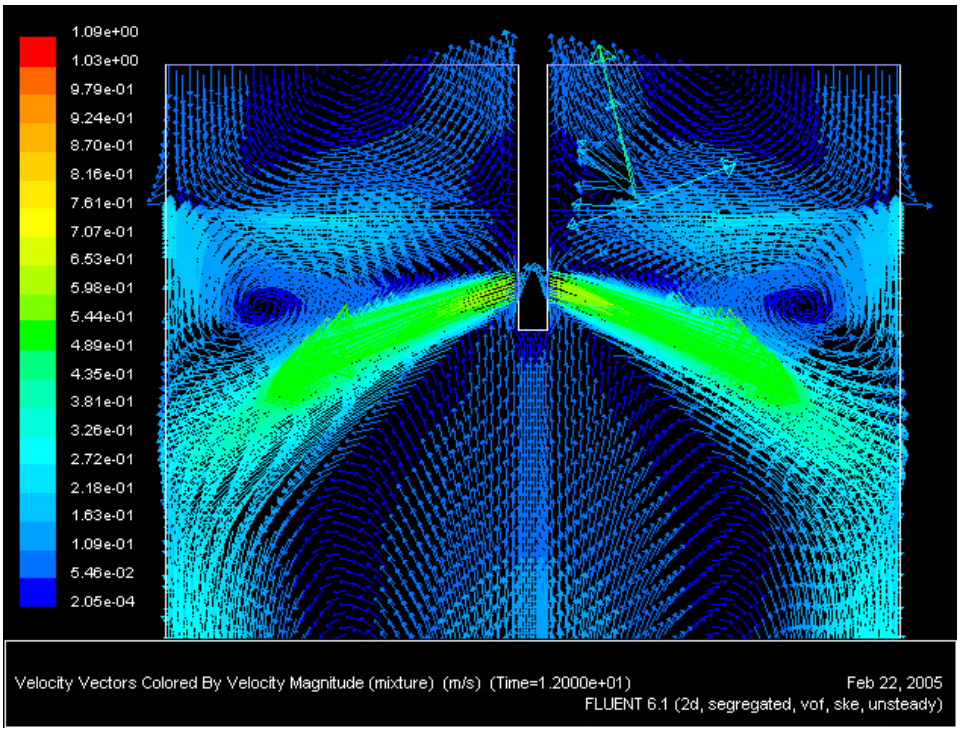

Figure 7. Velocity vectors for Case 3 in the upper water model region.

Corresponding numerical meniscus profiles for Cases 3, 7 and 9 are shown in Figures 8, 9 and 10. In Figure 8 is depicted the meniscus profile in the right part of the water mold for Case 3. In Case 3 the SEN submergence depth is rather low, 0.05 m, and the water volumetric flow rate is high, namely 5.83×10^{-4} m^3 s^{-1}. The water in contact with the narrow wall has a high level due to the ascending flow of the water upper recirculation roll. The lowest water level is present at two-thirds of the distance between the SEN and the narrow wall. Near the SEN the water level rises and suddenly decreases because the water flow is directed below. This behavior of the meniscus profile is at least qualitatively corroborated with the water model experimental results shown in Figure 3.

Figure 9 shows the meniscus profile for the Case 7 obtained by means of numerical simulations. Case 7 is the opposite to Case 3. In Case 7 the SEN submergence depth is the highest considered in the experiments, i.e. 0.09 m, and the water volumetric flow rate is the lowest, namely 3.50×10^{-4} m^3 s^{-1}. Qualitative agreement with the experimental results shown in Figure 4 is observed in the water in contact with the narrow wall of the mold and also near the SEN. In both figures it can be observed that the water level near the SEN is above the water level near the narrow wall. This is explained by the low volumetric flow rate which yields a small ascending flow near the narrow wall of the mold. Near the SEN, the downward suction of the water jet is small, therefore the water level in this site is high.

Figure 10 shows the numerical meniscus profile for Case 9, and the corresponding experimental profile is depicted in Figure 5. In Case 9 the highest SEN submergence depth and the highest water volumetric flow rate are considered. The site where the water level is minimum is displaced towards the center of the region considered, as is expected due to the high volumetric flow rate.

From the experimental and numerical results, one can appreciate that the meniscus strongly depend on the water volumetric flow rate and from the SEN submergence depth. Assuming that the similarity criterion between the water model and the real steel caster guarantees similar dynamic behavior in both fluids, then one can expect that the same parameters affect in the same way the meniscus profile of molten steel in the continuous casting mold.

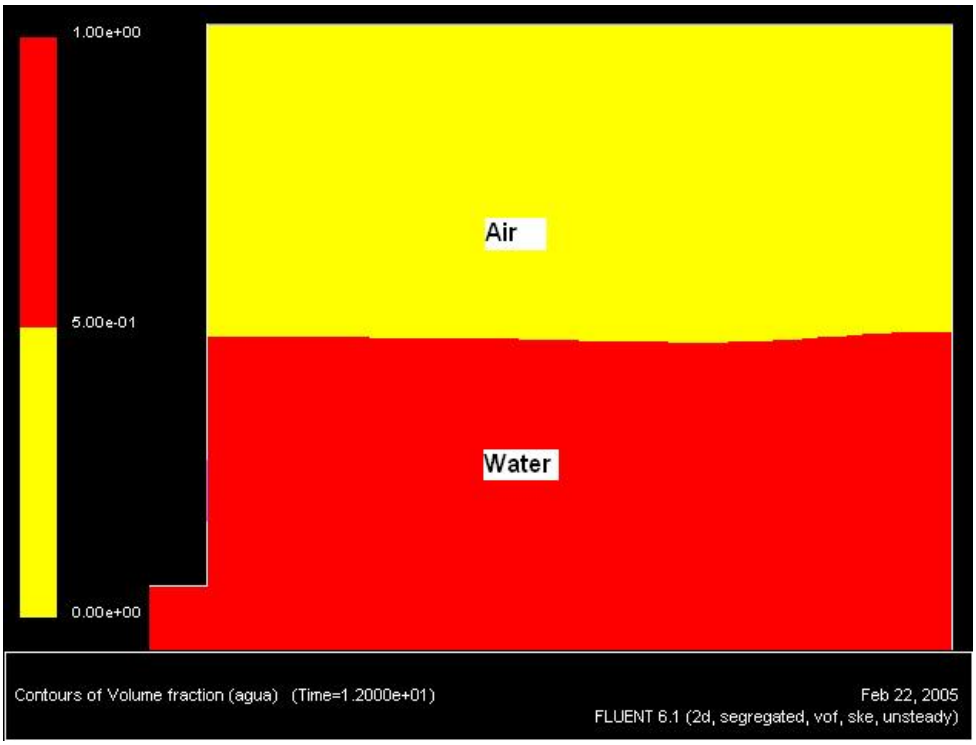

Figure 8. Meniscus profile for Case 3 in the right section of the mold.

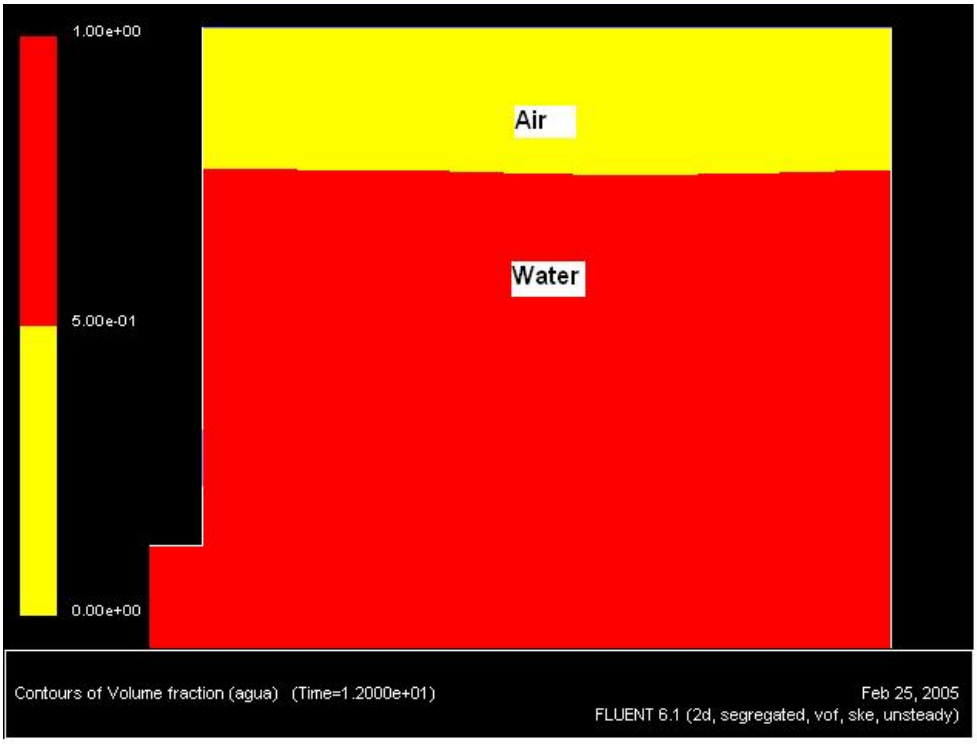

Figura 9. Meniscus profile for Case 7 in the right section of the mold.

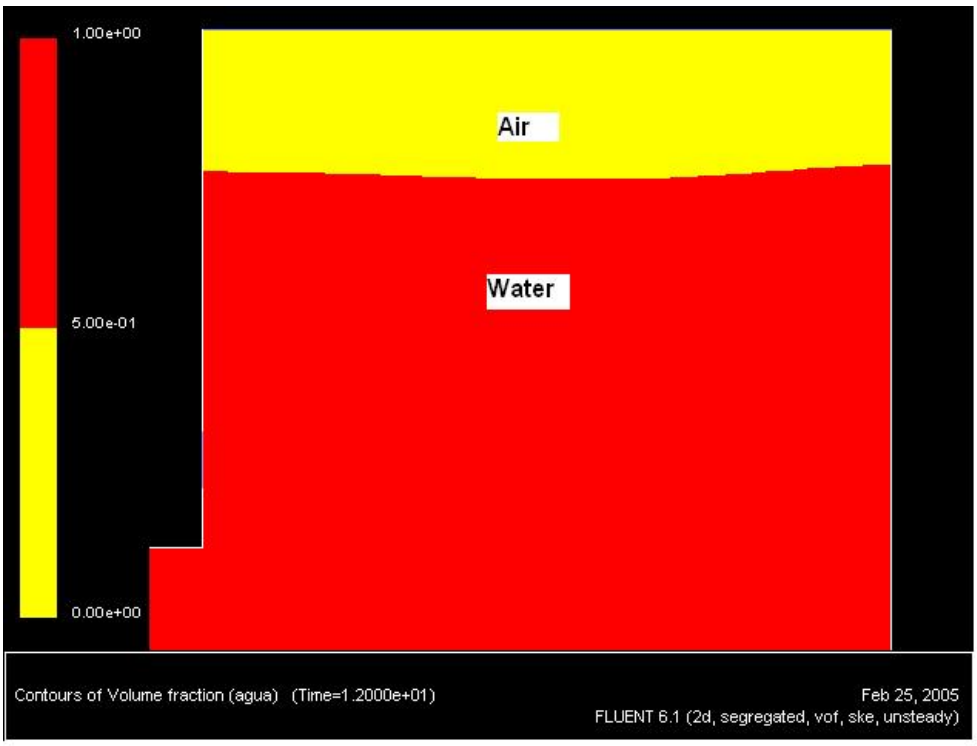

Figure 10. Meniscus profile for Case 9 in the right section of the mold.

Numerical simulations were conducted in order to study the influence of the SEN submergence depth and the water volumetric flow rate on the velocity distributions in the meniscus. To do this, an imaginary horizontal line along the meniscus located 0.005 m below the initial water level was considered. Results for the velocity magnitudes are depicted in Figures 11 and 12.

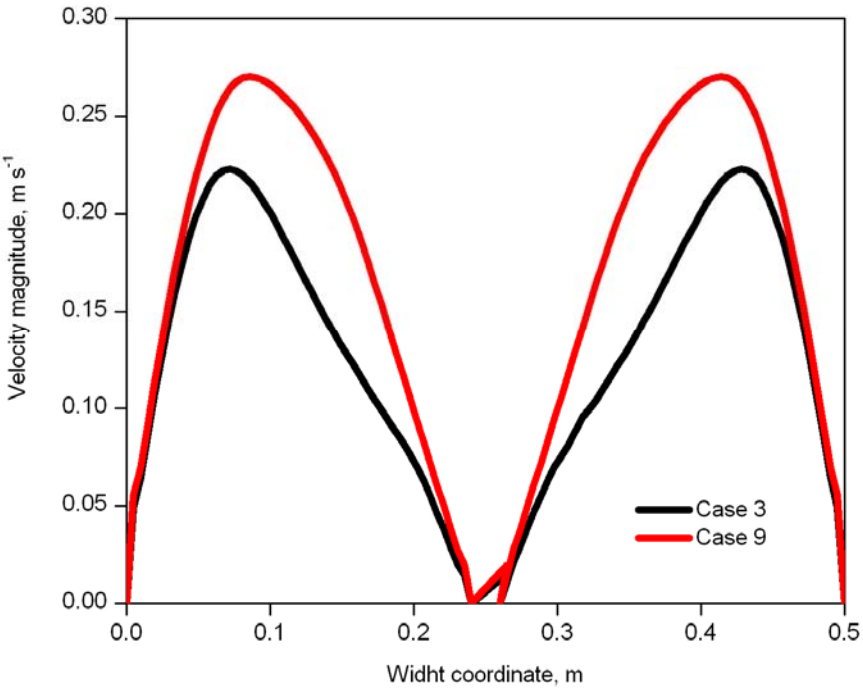

Figure 11. Velocity magnitude as a function of SEN submergence depth.

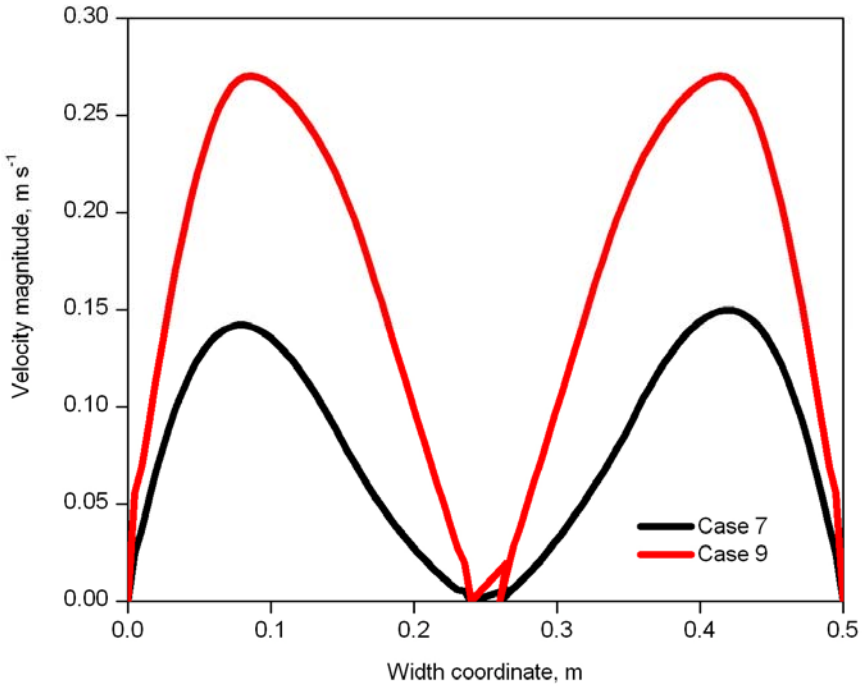

Figure 12. Velocity magnitude as a function of the water volumetric flow rate.

Figure 11 shows the distributions of the velocity magnitudes along the mold width for the imaginary line considered. In Case 3 the SEN submergence depth is 0.05 m, whilst in Case 9 the SEN submergence depth is 0.09 m. The water volumetric flow rate in both cases is 5.83×10^{-4} m^3 s^{-1}. It is evident than the velocity magnitude near the meniscus is higher for a higher SEN submergence depth. The effect of the water volumetric flow rate on the velocity magnitudes are seen in Figure 12. Both Case 7 and Case 9 have submergence depth of 0.09 m, and the flow rate for Case 7 is 3.50×10^{-4} m^3 s^{-1}, whilst for Case 9 the flow rate is 5.83×10^{-4} m^3 s^{-1}. From Figure 12 one can see that the influence of the water volumetric flow rate on the magnitude of velocities are stronger than that of the SEN submergence depth. Comparing the experimental results of Figures 3-5 and the numerical results of Figures 8-10 with Figures 11-12, it can be observed that the region of the meniscus in which the velocity magnitude is a maximum corresponds with that region of the meniscus where the water level is minimal.

In a previous work [5] the authors of the present work have reported a statistical analysis of the experimental data for each sensor position and for each case considered in Table 1. The optimal position of the level sensor for control purposes was defined as that position which yields the minimum data spread. Basically, Miranda et. al conclude that the optimal position of the level sensor is displaced towards the SEN as the water volumetric flow rate is increased, and that the influence of the SEN submergence depth on the sensor optimal position is unclear. In terms of the results of this work, one can observe that the zone of the meniscus where the water level is minimal is also displaced towards the SEN as the volumetric flow rate is increased. So, apparently, the optimal sensor position for control purposes must be that were the water level reaches a minimal value.

5. CONCLUSIONS

Physical and numerical simulations have been carried out in order to determine the meniscus profile in a continuous casting water model. Agreement between both results confirm that nowadays CFD numerical simulation is a valuable tool for study the molten steel flow in the continuous casting process. Water volumetric flow rate, in the case of physical models, or casting speed in the case of industrial casters, greatly affect the meniscus profile. In a lesser extent, the SEN submergence depth also affects the meniscus profile. The optimal sensor level position apparently is related with that region of the meniscus in which the water level or the molten steel level is minimal.

6. REFERENCES

1. Zhang, L., Thomas, B. State of the art in evaluation and control of steel cleanliness. *Met. Trans. B*., 43 (2003) 271-291.
2. Panaras, G.A., Theodorakakos., A., Bergeles, G. Numerical investigation of the free surface in a continuous steel casting mold model. *Met. Trans. B*, 29B (1998) 1117-1126.
3. Agnanostopoulos, J., Bergeles, G. Three-dimensional modeling of the flow and the interface surface in a continuous casting mold model. *Met. Trans. B*, 30B (1999) 1095-1105.
4. Dash, S.K, Mondal, S.S. Mathematical simulation of surface wave created in a mold due to submerged entry nozzle. Intl. J. Num. Meth. Heat & Fluid Flow., 14 (2004) 606-632.
5. Miranda, R., Barron, M.A., de Ita, A., Hoyos, L., Gonzalez, J. Optimization of the level sensor position for a continuous slab caster. *Proc. of 39th IAS IEEE Annual Meeting*. Seattle, WA, 3-7 October 2004.
6. Li, B., Tsukihasi, F. Vortexing flow patterns in a water model of slab continuous casting mold. *ISIJ Intl.*, 45 (2005) 30-36.
7. Bird, R.B., Stewart, W.E., Lightfoot, E.N. *Transport Phenomena*. Wiley, Second Edition 2002, USA, pp. 846-847.
8. Ferziger, H.J., Peric, M. *Computational Methods for Fluid Dynamics*, Springer, Second Edition 1999, Germany.
9. Fluent, Inc. *User Guide*, Chapter 20 (2003) 20-4.